Journal of Molecular Catalysis A: Chemical 331 (2010) 15–20

Contents lists available at ScienceDirect

Journal of Molecular Catalysis A: Chemical

journal homepage: www.elsevier.com/locate/molcata

Editor's Choice paper

Citric acid assisted solvothermal synthesis of $BiFeO_3$ microspheres with high visible-light photocatalytic activity

Yuning Huo*, Yi Jin, Ya Zhang

Department of Chemistry, Shanghai Normal University, 100 Guilin R., Shanghai 200234, PR China

ARTICLE INFO

Article history:
Received 1 April 2010
Received in revised form 29 July 2010
Accepted 7 August 2010
Available online 14 August 2010

Keywords:
$BiFeO_3$ photocatalyst
Solvothermal preparation
Citric acid
Visible light
Methylene blue (MB)

ABSTRACT

A novel $BiFeO_3$ photocatalyst in the shape of uniform microspheres has been synthesized by solvothermal process assisted with chelating effect of citric acid. The higher photoactivity of this catalyst than that of $BiFeO_3$ via solid-state reaction for methylene blue (MB) degradation under visible-light irradiation is owing to the high crystallization of perovskite-type $BiFeO_3$, high surface area with hollow structure, narrow band gap energy of 2.1 eV, and the promotion of separation of photo-induced electrons and holes. Additionally, no decrease of activity after being reused repetitively for five times is indicative of the high hydrothermal stability of $BiFeO_3$ particles without crystal phase transformation.

1. Introduction

Due to the increasing environmental pollution in recent years, the degradation of organic pollutants has generated broad interest of photocatalysis for both scientific understanding and potential applications [1,2]. The TiO_2 photocatalyst is widely employed in the environmental cleaning by degrading organic pollutants and hydrogen production by splitting water, due to their excellent photochemical stability, low cost, and non-toxicity [3,4]. However, the large band gap energy (3.2 eV) of TiO_2 severely restricts its absorption in the visible-light region, although many efforts have been devoted to extend optical response of TiO_2 into visible-light region and to improve the quantum efficiency of photocatalysis by modifying TiO_2 with metals, non-metals, semiconductor oxides, and/or photo-sensitizers [5–8]. The development of novel non-titania semiconductors with strong absorbance for broad ranged visible lights represents a current trend in photocatalysis [9,10]. Bismuth-oxide-based photocatalysts are attractive materials [11–14], however, Bi_2O_3 shows deactivation due to formation of carbonate and this limitation is only partially solved via formation of nanocomposites. Bi-contained oxides often offer interesting optical properties for photocatalytic applications [15–17] Recently, the perovskite-type $BiFeO_3$ photocatalyst (BFO) has attracted considerable attention owing to the narrow band-gap energy (2.1 eV) [18–21], and high chemical stability [17,22], in addition to acting as a well-known multiferric compound, which exhibiting a coexistence of simultaneous ferroelectric and magnetic order parameters [23,24]. Various methods have been developed for the preparation of micrometer- and nanometer-sized $BiFeO_3$ crystallites, such as conventional solid-state reaction [25,26], co-precipitation [27], sol–gel process [28–30], and hydrothermal route [21,31–33]. However, in general, it is still inconvenient to prepare $BiFeO_3$ compounds without impurity phases due to the low stability of Bi atom in perovskite $BiFeO_3$ [34], and it is not easy to achieve the structure-controllable $BiFeO_3$ with high surface area [16,35]. Furthermore, the synthesis of $BiFeO_3$ sometimes is based on complex solution processes and involves toxic precursors [28,36]. Therefore, it is essential to develop an environmental-friendly method to obtain the pure $BiFeO_3$ photocatalyst with controllable structure. As we know, the solvothermal process has emerged as a powerful method for the fabrication of inorganic materials, because of their great synthetic flexibility and controlled growth of small-scale crystallites [37,38]. In this paper, we report a solvothermal synthesis route, which involves no toxicants and is carried out at lower temperature, to prepare pure $BiFeO_3$ crystals in the shape of uniform microspheres with high surface area. The correlation between controllable structure of $BiFeO_3$ and high photoactivity together with durability under visible-light irradiations is investigated.

2. Experiment

2.1. Catalyst preparation

All source chemicals (analytical grade) are purchased from Shanghai Chemical Regents Company and used without further purification. In a typical run of synthesis, 0.040 mol/L bismuth

* Corresponding author. Tel.: +86 21 64322642; fax: +86 21 64322272.
E-mail address: Huoyuning@shnu.edu.cn (Y. Huo).

1381-1169/$ – see front matter © 2010 Elsevier B.V. All rights reserved.
doi:10.1016/j.molcata.2010.08.009

nitrate ($Bi(NO_3)_3{\cdot}5H_2O$), iron nitrate ($Fe(NO_3)_3{\cdot}9H_2O$) and citric acid with a molar ratio of 1:1:1 are added into the mixture solution of 10.0 mL glycerol and 30.0 mL ethanol. It has been found that $Bi(NO_3)_3{\cdot}5H_2O$ is very difficult to be dissolved without glycerol. After ultrasonic dispersion for 10 min, the mixed solution becomes clear and presents brownish red color. Then, the solution is poured into a 50.0 mL stainless-steel Teflon-lined autoclave for the solvothermal reaction with a filling capacity of 80%. After being sealed, the autoclave is heated up to a certain temperature and held for the desired time, and then is cooled to room temperature naturally. The products are filtered and washed with both distilled water and anhydrous ethanol several times, followed by being dried at 353 K for 12 h and being calcined at expected temperature for 4 h. The as-prepared samples are denoted as BFO-*X*–*Y*–*Z*, where *X*, *Y* and *Z* refer to the alcoholysis time in hours (*X*), alcoholysis temperature in K (*Y*) and calcination temperature in K (*Z*), respectively. For comparison, the $BiFeO_3$ prepared without citric acid under the same condition of BFO-24–433–773 is expressed as BFO-NCA, and the conventional $BiFeO_3$ is synthesized via solid-state reaction at 1073 K for 5 h [26] and denoted as BFO-SSR. The P25 TiO_2 is commercially available and used without further treatment.

2.2. Characterizations

The sample composition is determined by inductively coupled plasma (ICP, Varian VISTA-MPX). The catalyst structure is investigated by X-ray diffraction (XRD, Rigacu Dmax-3C, Cu Ka radiation). The grain size is calculated by using Scherrer equation based on the principal XRD peak. Surface morphology and particle size are observed through scanning electron microscopy (SEM, JEOL JSM-6380LV) and transmission electronic microscopy (TEM, JEM-2010). N_2 adsorption–desorption isotherms are measured on a Quantachrome NOVA 4000e at 77 K. The Brunauer–Emmett–Teller (BET) method is used to calculate the specific surface area (S_{BET}). The thermal stability is investigated by a thermogravimetric analyzer (DTG-60H, 10 °C/min heating rate). The light absorption ability is analyzed by UV–vis diffuse reflectance spectra (DRS, MC-2530).

2.3. Activity test

The photocatalytic degradation of methylene blue (MB) is carried out at 303 K in a self-designed 100 mL glassy reactor containing 0.050 g catalyst and 50.0 mL of 10.0 mg/L MB aqueous solution. The reaction system is stirred vigorously (>800 rpm) to eliminate diffusion effect on the reaction kinetics. Keeping the mixture for more than 1 h to reach adsorption equilibrium, the photocatalytic reaction is initiated by irradiating with a 500 W Xenon lamp (CHF-XM500, light intensity = 600 mW/cm^2) located at 18 cm above the solution. To make sure that the photocatalytic reaction is really driven by visible-light, all the UV lights with wavelength lower than 420 nm are removed by a glass filter (JB-420). Each run of the reactions is lasted for 4 h and the MB left in the solution is analyzed by a UV spectrophotometer (UV 7504/PC) at its characteristic wavelength (λ = 665 nm) [39]. Little organic byproducts have been identified by HPLC–MS after the reaction for 4 h. Preliminary tests show that there is a good linear relationship between the light absorbance and the concentration of organic compounds. Meanwhile, experimental results also confirm that only less than 9.0% MB is adsorbed by catalysts after reaction for 4 h without light irradiation (Table 1), and only 6.0% MB is decomposed under light irradiation in the absence of catalysts, and thus could be neglected in comparison with the photocatalysis process. The reproducibility of the results is checked by repeating the experiments at least three times and is found to be within acceptable limits (±5%). The durability of catalyst is measured according to the following procedure. After each run of photocatalysis reactions, the photocatalyst is separated from aqueous solution by centrifugation, washed with distilled water for three times and dried at 373 K for 12 h. Then, each recycling test is conducted under the same conditions for 4 h and the MB degradation yield is determined to show the change of activity.

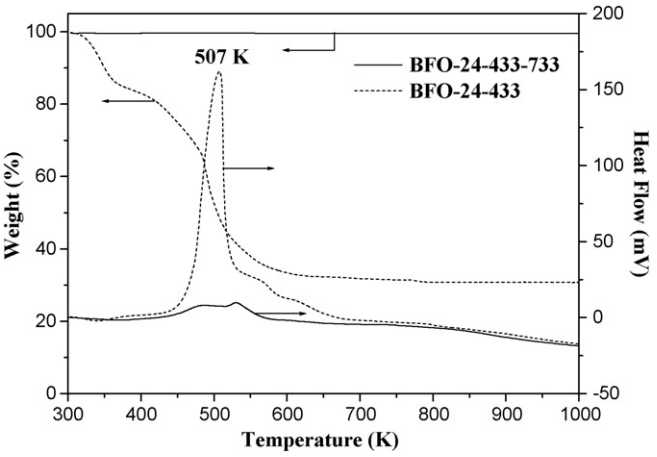

Fig. 1. TG-DTA curves of BFO-24–433 and BFO-24–433–773 samples.

3. Results and discussion

The TG-DTA curves in Fig. 1 reveal that BFO-24–433 sample exhibits an exothermic peak around 507 K with weight loss around 30%, while the BFO-24–433–773 displays no significant weight loss and exothermic peaks, suggesting the complete removal of organic residues after the calcination. According to the ICP results, the Bi/Fe molar ratio in BFO-24–433–773 determines the formation of $BiFeO_3$. XRD patterns in Fig. 2 further demonstrate that both BFO-24–433–773 and BFO-SSR have the typical perovskite-type $BiFeO_3$ with *R3c* rhombohedral structure (JCPDS 86-1518), as shown in Scheme 1 [32,40], and no other crystal phases can be observed in the diffraction patterns. However, based on the Scherrer equation ($D = K\lambda/\beta\cos\theta$), the BFO-24–433–773 has much smaller crystallite size than BFO-SSR (see Table 1). It could be attributed that the rate of crystal nucleation is greater than that of crystal growth during the solvothermal process, and thus leads to smaller crystal size and lower aspect ratio of the crystal than those resulted from fast crystal growth under solid-state reaction at high temperature [32]. Accordingly, the BFO-24–433–773 reveals much higher S_{BET} than

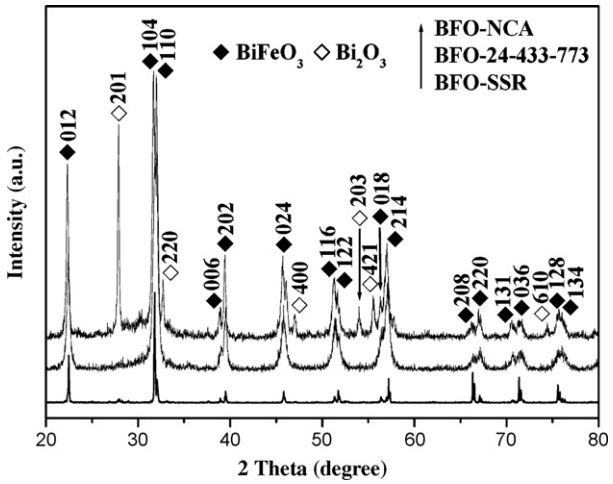

Fig. 2. XRD patterns of $BiFeO_3$ samples synthesized via with different routes.

Table 1
Crystallite size, specific surface area and photoactivity of different photocatalysts.

Catalyst	Crystallite size[a] (nm)	S_{BET} (m^2/g)	Degradation[b] (%)	Adsorption[c] (%)
BFO-6–433–773	14.0	18.0	66	7
BFO-12–433–773	23.6	16.4	71	6
BFO-24–433–773	29.2	15.3	86	6
BFO-48–433–773	44.4	12.2	80	6
BFO-24–393–773	14.8	16.8	66	8
BFO-24–473–773	36.8	10.2	55	5
BFO-24–433–673	13.3	28.1	56	8
BFO-24–433–873	53.5	7.2	70	4
BFO-NCA	37.4	4.2	48	3
BFO-SSR	78.5	1.2	12	3
P 25 TiO_2	20.0	45.0	10	8

[a] Calculated by Scherrer equation.
[b] Reaction conditions: 0.050 g catalyst, 50.0 mL solution of 10.0 mg/L MB, reaction temperature = 303 K, stirring rate > 800 rpm, one 500 W Xe lamp (light intensity = 600 mW/cm^2, wavelength > 420 nm), reaction time = 4 h.
[c] Same as above conditions without light irridiations.

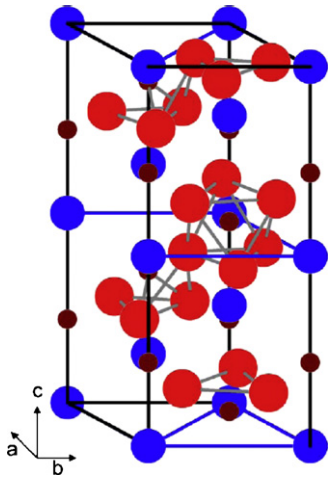

Scheme 1. Structure of *R3c* rhombohedral cell in perovskite-type $BiFeO_3$ (● = Bi, ● = O, ● = Fe). (For interpretation of the references to color in this figure legend, the reader is referred to the web version of the article.)

BFO-SSR, as shown in Table 1. On the other hand, comparing to the pure $BiFeO_3$ crystal phase in BFO-24–433–773, BFO-NCA sample without citric acid shows significant impurity Bi_2O_3 crystal phase (JCPDS 27-0050), besides the larger crystal size of $BiFeO_3$ crystal.

Fig. 3(a) shows the typical SEM morphology for BFO-24–433–773 sample, which presents well-dispersed microspheres with the uniform diameter of about 1.5 μm, and the inserted TEM morphology confirms the hollow structure of microspheres with the shell of about 0.2 μm thickness. However, the BFO-NCA microspheres exhibit wide distribution of particle size and the obvious agglomeration of particles, leading to the smaller S_{BET} than that of BFO-24–433–773 (Table 1). It can be attributed to the attachment of citrate groups on the surface of $BiFeO_3$ crystals during the solvothermal reaction, which could efficiently prevent from particle aggregating into large crystals [41]. Additionally, the removal of organic compounds during the calcination process may result in the hollow architecture.

Based on above discussions, speculated process for the formation of catalysts can be brought out as the following equations. Firstly, Bi^{3+} and Fe^{3+} are produced after $Bi(NO_3)_3$ and $Fe(NO_3)_3$ dissolved into the solution mixed with glycerol and ethanol (Eqs. (1) and (2)), respectively. In the case of citric acid, Bi^{3+} can be easily combined with citric acid via the chelating effect prior to Fe^{3+} (Eq. (3)), owing to the much higher stability constant than Fe^{3+} complex [42,43]. Then, Bi^{3+} will be released slowly and gradually converted into $Bi(OH)_3$ via the alcoholysis reaction (Eq. (4)) during the solvothermal process. Then, the simultaneously formed $Fe(OH)_3$ (Eq. (5)) could react with $Bi(OH)_3$ to form the uniform $BiFeO_3$ precipitates by the condensation effect (Eq. (6)), and to further generate the well-dispersed $BiFeO_3$ microspheres with uniform particle sizes. However, in the absence of citric acid, owing to no chelating effect existed and the higher pH value [44,45], the greatly accelerated alcoholysis process of Bi^{3+} occurs rapidly (Eq. (7)), resulting in the non-uniform crystal growth and larger crystal size of $BiFeO_3$ particles with obvious agglomeration. Meanwhile, the formation of unstable Bi_2O_3 crystal can be also caused easily (Eq. (8)).

$$Bi(NO_3)_3 \rightarrow Bi^{3+} + 3NO_3^- \quad (1)$$

$$Fe(NO_3)_3 \rightarrow Fe^{3+} + 3NO_3^- \quad (2)$$

$$Bi^{3+} + C_6O_7H_8 \rightarrow [C_6O_7H_5]^{3-}Bi^{3+} + 3H^+ \quad (3)$$

$$[C_6O_7H_5]^{3-}Bi^{3+} + 3OH^- \rightarrow Bi(OH)_3 + [C_6O_7H_5]^{3-} \quad (4)$$

$$Fe^{3+} + 3OH^- \rightarrow Fe(OH)_3 \quad (5)$$

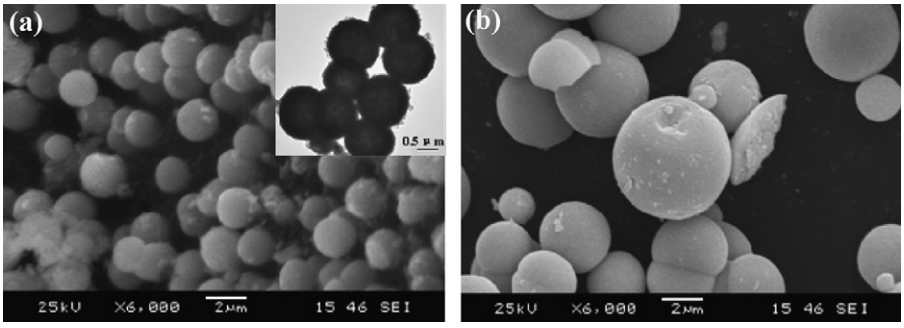

Fig. 3. SEM morphologies of (a) BFO-24–433–773 with inserted TEM image and (b) BFO-NCA.

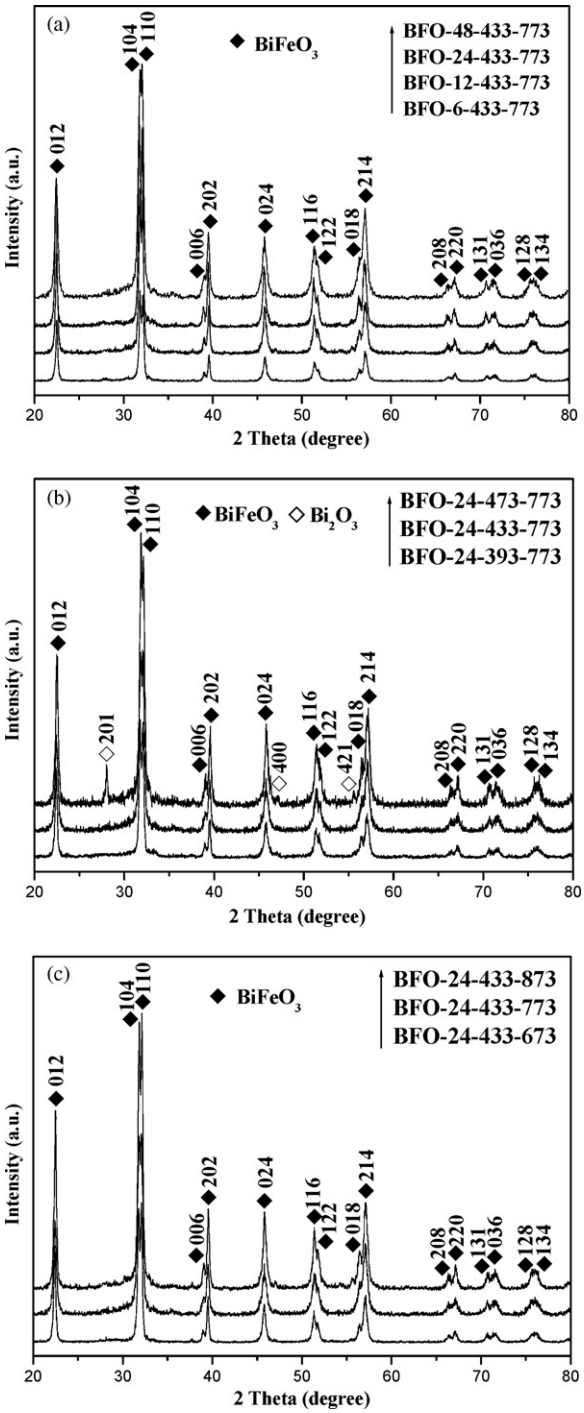

Fig. 4. XRD patterns of BFO samples prepared under different (a) alcoholysis time, (b) alcoholysis temperature, and (c) calcination temperature.

$$Bi(OH)_3 + Fe(OH)_3 \rightarrow BiFeO_3 + 3H_2O \quad (6)$$

$$Bi^{3+} + 3OH^- \rightarrow Bi(OH)_3 \quad (7)$$

$$2Bi(OH)_3 \rightarrow Bi_2O_3 + 3H_2O \quad (8)$$

Fig. 4 and Table 1 present the XRD patterns, crystallite size and S_{BET} for BFO-*X*–*Y*–*Z* samples prepared under different conditions, respectively. The increased alcoholysis time results in the enhanced crystallization of perovskite-type $BiFeO_3$ with gradually increased crystallite size and decreased S_{BET}, owing to the growth of crystals during the solvothermal process. Meanwhile, the elevated temperature of both alcoholysis and calcination

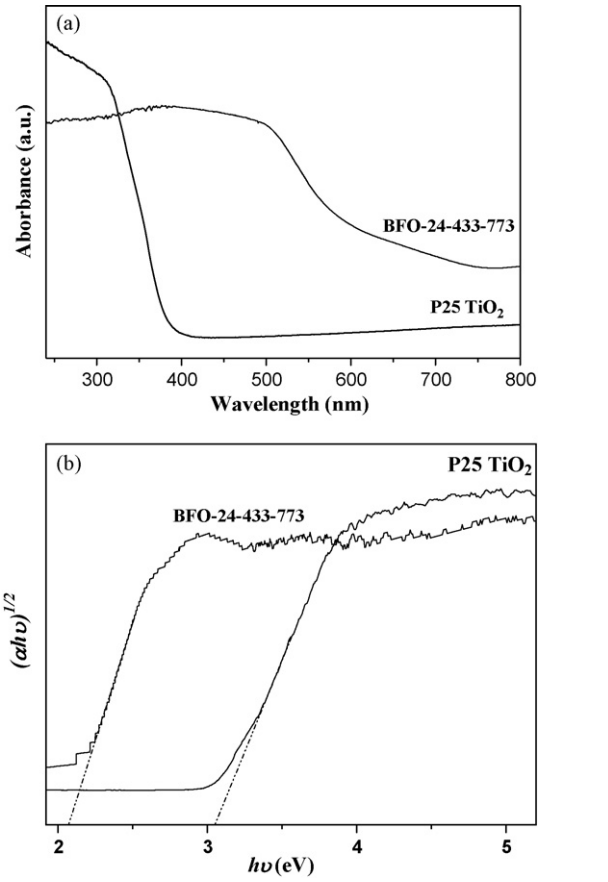

Fig. 5. UV–vis DRS spectra (a) and the optical absorption edges (b) of P25 TiO_2 and BFO-24–433–773 samples.

can significantly improve the crystallization of $BiFeO_3$ with the enlarged crystallite size and decrease the specific surface area owing to the crystal growth and agglomeration of particles, especially the abruptly decreased S_{BET} of BFO-24–433–873. In addition, the impurity of Bi_2O_3 crystal generated in BFO-24–473–773 is possibly due to no chelating effect from decomposition of citric acid and the rapid alcoholysis process of Bi^{3+} at high alcoholysis temperature.

Fig. 5(a) exhibits UV–vis DRS spectra of both BFO-24–433–773 and P25 TiO_2. Comparing to P25 TiO_2 without any absorption of visible-light, BFO-24–433–773 has strong visible-light absorption in wide visible region up to about 600 nm, indicating the much higher utilization of visible light of $BiFeO_3$ than TiO_2. According to the UV–vis DRS spectra, the band-gap energy can be calculated by using $(\alpha h\upsilon)^n = k(h\upsilon - E_g)$, where α is the absorption coefficient, k is the parameter that related to the effective masses associated with the valence and conduction bands, n is 1/2 for a direct transition, $h\upsilon$ is the absorption energy, and E_g is the band-gap energy [46–47]. Plotting $(\alpha h\upsilon)^{1/2}$ *vs* $h\upsilon$ gave the extrapolated intercept corresponding to the E_g values. From the optical absorption edges (Fig. 5(b)), the E_g of TiO_2 and BFO-24–433–773 can be determined as 3.1 and 2.1 eV, respectively, in accordance with the previous reports [21]. The narrow E_g of BFO-24–433–773 is resulted from the inherent conduction and valance bands of $BiFeO_3$, relating to defect states due to oxygen vacancies [48,49].

The photodegradation properties of MB, a typical organic pollutant in the wastewater from dyeing industries, for all samples under the irradiation of visible lights (wavelength > 420 nm) are summarized in Table 1. P25 TiO_2 shows very low photodegradation of MB since it is not activated by visible lights due to its big energy gap

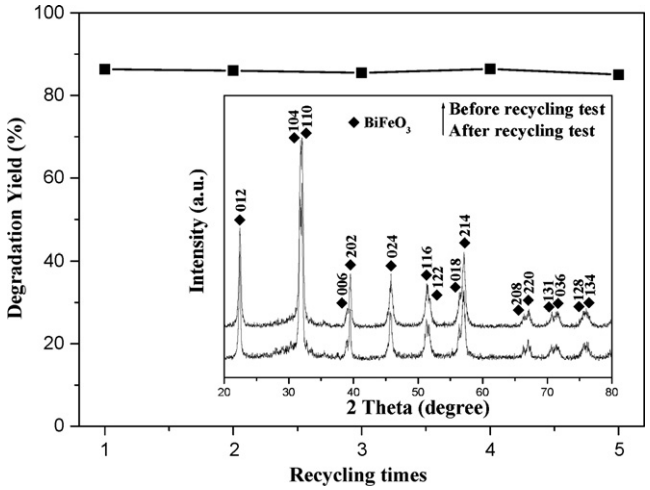

Fig. 6. Recycling tests of BFO-24–433–773 catalyst with inserted XRD patterns before and after recycling test. Reaction conditions: 0.050 g catalyst, 50.0 mL solution of 10.0 mg/L RhB, reaction temperature = 303 K, stirring rate > 800 rpm, one 500 W Xe lamp (light intensity = 600 mW/cm^2, wavelength > 420 nm). Each run of photocatalytic reactions lasted for 4 h.

(3.1 eV). According to the average diffusion time (τ) from bulk to surface for randomly generated charge carriers, $\tau = r^2\pi^2 D$, where r is the grain radius and D is the diffusion coefficient of the carrier [45], the large crystallite size of BFO-SSR will lead to the long diffusion time and thus the greatly enhanced recombination opportunities of photo-generated electrons and holes will be greatly increased, resulting in the low photoactivity [50]. Additionally, the low S_{BET} of BFO-SSR results in the less absorption of reactants and is not favorable for the degradation process. All the BFO samples prepared via solvothermal process present much higher activity than P25 TiO_2, since the narrow band gap (2.1 eV) of $BiFeO_3$ crystal leads to the efficient utilization of visible light, and the transfer of holes in valence band becomes easy by the formation of hybrid Bi 6s and O 2p orbital [19]. The activity is also much higher than BFO-SSR owing to the smaller crystallite size and larger S_{BET}, resulting in the greatly enhanced separation efficiency of photo-induced electrons and holes, besides the increased reactive sites [50–52]. At the same time, the hollow structure is favorable for the improvement of the light utilization and the access of reactant molecules into internal part of catalysts to enhance the efficiency of photocatalysis reactions. The greatly increased photoactivity of BFO-24–433–773 than that of BFO-NCA indicates that the key role of citric acid for chelating Bi^{3+} during the solvothermal reactions leads to the formation of uniform microspheres with small crystallite size, high S_{BET} and no particle agglomeration, and the inhibition of forming impurity Bi_2O_3 crystal phase, which is unstable during the photocatalysis process.

The preparation conditions also have significant effects on the degradation activities. The alcoholysis time increased from 6 to 24 h leads to the promotion of photoactivity, mainly due to the improved crystallization of $BiFeO_3$ crystals. However, further increased time to 48 h results in the small S_{BET}, causing the slightly decreased activity. With the elevated alcoholysis temperature from 393 to 433 K, the increased crystallization of $BiFeO_3$ crystals enhances the photocatalysis activity. However, the obviously decreased activity at 473 K can be attributed to the unstable Bi_2O_3 crystals formed [53,54], which are decomposed easily during the photocatalysis reactions, besides the decreased S_{BET} with larger crystallite size. The calcination temperature also influences the crystallization significantly. The promoted photoactivity of $BiFeO_3$ samples with the calcination temperature elevated from 673 to 773 K, is due to the well crystallization of $BiFeO_3$ crystals, however, further increased temperature will cause the declined activity mainly owing to the reduction of S_{BET}.

In addition to the high photoactivity, the durability of BFO-24–433–773 is also displayed in Fig. 6. After being reused for five times, no obvious decrease of photocatalytic activity can be observed, which is attributed to the excellent hydrothermal stability of $BiFeO_3$ microspheres. The inserted XRD patterns further confirm there is no significant transformation of $BiFeO_3$ crystal phase after recycling tests, indicative of the stability of $BiFeO_3$ crystals.

4. Conclusion

A novel approach for $BiFeO_3$ photocatalysts via solvothermal preparation with the chelating effect of citric acid has been developed. This catalyst exhibits high crystallization, large surface area with uniform shape of hollow microspheres and narrow band gap, leading to the high photocatalytic activity for MB degradation under visible-light irradiations. Furthermore, the hydrothermal stability of $BiFeO_3$ particles without crystal phase transformation results in the repetitive reuse, which is favorable for the potential applications.

Acknowledgments

This work is supported by National Natural Science Foundation of China (20937003), Key Laboratory of Resource Chemistry of Ministry of Education, Shanghai Government (S30406, 07dz22303, 0852nm01000, 09YZ162, 09JC1411400, 10230711600), State Key Laboratory of High Performance Ceramics and Superfine Microstructures (SKL200909SIC) and Shanghai Normal University (DZL807, SK200838).

References

[1] A.J. Esswein, D.G. Nocera, Chem. Rev. 107 (2007) 4022–4047.
[2] M. Anpo, M. Takeuchi, J. Catal. 216 (2003) 505–516.
[3] X.B. Chen, S.S. Mao, Chem. Rev. 107 (2007) 2891–2959.
[4] H.J. Zhang, G.H. Chen, D.W. Bahnemann, J. Mater. Chem. 19 (2009) 5089–5121.
[5] K. Nagaveni, M.S. Hegde, G. Madras, J. Phys. Chem. B 108 (2004) 20204–20212.
[6] H.X. Li, J.X. Li, Y.N. Huo, J. Phys. Chem. B 110 (2006) 1559–1565.
[7] J.C. Yu, L. Wu, J. Lin, P. Li, Q. Li, Chem. Commun. (2003) 1552–1553.
[8] D. Zhao, C.C. Chen, Y.F. Wang, W.H. Ma, J.C. Zhao, T. Rajh, L. Zang, Environ. Sci. Technol. 42 (2008) 308–314.
[9] M.D. Hernández-Alonso, F. Fresno, S. Suárez, J.M. Coronado, Energy Environ. Sci. 2 (2009) 1231–1257.
[10] T. Kako, Z.G. Zou, M. Katagiri, J.H. Ye, Chem. Mater. 19 (2007) 198–202.
[11] A. Hameed, T. Montini, V. Gombac, P. Fornasiero, J. Am. Chem. Soc. 130 (2008) 9658–9659.
[12] J. Eberl, H. Kisch, Photochem. Photobio. Sci. 7 (2008) 1400–1406.
[13] A. Hameed, V. Gombac, T. Montini, L. Felisari, P. Fornasiero, Chem. Phys. Lett. 483 (2009) 254–261.
[14] A. Hameed, V. Gombac, T. Montini, M. Graziani, P. Fornasiero, Chem. Phys. Lett. 472 (2009) 212–216.
[15] J.W. Tang, Z.G. Zou, J.H. Ye, Angew. Chem., Int. Ed. 43 (2004) 4463–4466.
[16] F. Gao, Y. Yuan, K.F. Wang, X.Y. Chen, F. Chen, J.M. Liu, Appl. Phys. Lett. 89 (2006) 1025061–1025063.
[17] Z.F. Bian, Y.N. Huo, Y. Zhang, J. Zhu, Y.F. Lu, H.X. Li, Appl. Catal. B 91 (2009) 247–253.
[18] F. Gao, X. Chen, K. Yin, S. Dong, Z. Ren, F. Yuan, T. Yu, Z. Zou, J.M. Liu, Adv. Mater. 19 (2007) 2889–2892.
[19] X.Y. Chen, T. Yu, F. Gao, H.T. Zhang, L.F. Liu, Y.M. Wang, Z.S. Li, Z.G. Zou, Appl. Phys. Lett. 91 (2007) 0221141–0221143.
[20] C.M. Cho, J.H. Noh, I.S. Cho, J.S. An, K.S. Hongw, J.Y. Kim, J. Am. Ceram. Soc. 91 (2008) 3753–3755.
[21] J.H. Luo, P.A. Maggard, Adv. Mater. 18 (2006) 514–517.
[22] S. Li, Y.H. Lin, B.P. Zhang, J.F. Li, C.W. Nan, J. Appl. Phys. 105 (2009) 0543101–0543105.
[23] T. Choi, S. Lee, Y.J. Choi, V. Kiryukhin, S.W. Cheong, Science 324 (2009) 63–66.
[24] N. Hur, S. Park, P.A. Sharma, J.S. Ahn, S. Guha, S.W. Cheong, Nature 429 (2004) 392–395.
[25] G.D. Achenbach, W.J. James, R. Gerson, J. Am. Ceram. Soc. 8 (1967) 437–438.
[26] M. Valant, A.K. Axelsson, N. Alford, Chem. Mater. 19 (2007) 5431–5436.
[27] S. Shetty, V.R. Palkar, R. Pinto, Pramana J. Phys. 58 (2002) 1027–1030.
[28] J.K. Kim, S.S. Kim, W.J. Kim, Mater. Lett. 59 (2005) 4006–4009.

[29] Z.C. Quan, H. Hu, S. Xu, W. Liu, G.J. Fang, M.Y. Li, X.Z. Zhao, J. Sol–Gel Sci. Technol. 48 (2008) 261–266.
[30] X. Wang, Y.G. Zhang, Z.B. Wu, Mater. Lett. 64 (2010) 486–488.
[31] C. Chen, J. Cheng, S. Yu, L.J. Che, Z.Y. Meng, J. Cryst. Growth 291 (2006) 135–139.
[32] J.T. Han, Y.H. Huang, X.J. Wu, C.L. Wu, W. Wei, B. Peng, W. Huang, J.B. Goodenough, Adv. Mater. 18 (2006) 2145–2148.
[33] S. Li, Y.H. lin, B.P. Zhang, C.W. Nan, Chin. J. Inorg. Chem. 26 (2010) 495–499.
[34] W. Sakamoto, A. Iwata, T. Yogo, J. Appl. Phys. 104 (2008) 1041061–1041068.
[35] X.Y. Zhang, C.W. Lai, X. Zhao, D.Y. Wang, J.Y. Dai, Appl. Phys. Lett. 87 (2005) 1431021–1431023.
[36] J. Chen, X.R. Xing, A. Watson, W. Wang, R.B. Yu, J.X. Deng, L. Yan, C. Sun, X.B. Chen, Chem. Mater. 19 (2007) 3598–3600.
[37] L.H. Zhuo, J.C. Ge, L.H. Cao, B. Tang, Cryst. Growth Des. 9 (2009) 1–6.
[38] B. Mazumder, P. Chirico, A.L. Hector, Inorg. Chem. 47 (2008) 9684–9690.
[39] M. Mrowetz, W. Balcerski, A.J. Colussi, M.R. Hoffmann, J. Phys. Chem. B 108 (2004) 17269–17273.
[40] J. Prado-Gonjal, M.E. Villafuerte-Castrejon, L. Fuentes, E. Moran, Mater. Res. Bull. 44 (2009) 1734–1737.
[41] J. Liu, Z.K. Sun, Y.H. Deng, Y. Zou, C.Y. Li, X.H. Guo, L.Q. Xiong, Y. Gao, F.Y. Li, D.Y. Zhao, Angew. Chem. Int. Ed. 48 (2009) 5875–5879.
[42] T.B. Field, J.L. Mccourt, W.A.E. Mcbryde, Can. J. Chem. 52 (1974) 3119–3124.
[43] W. Szczepaniak, M. Ren, Talanta 33 (1986) 371–373.
[44] M. Popa, S. Preda, V. Fruth, K. Sedlácková, C. Balázsic, D. Crespo, J.M. Calderón-Moreno, Thin Solid Films 517 (2009) 2581–2585.
[45] M. Shang, W.Z. Wang, S.M. Sun, L. Zhou, L. Zhang, J. Phys. Chem. C 112 (2008) 10407–10411.
[46] M. Yoon, M. Seo, C. Jeong, J.H. Jang, K.S. Jeon, Chem. Mater. 17 (2005) 6069–6079.
[47] L. Li, Y. Yang, X. Huang, G. Li, L. Zhang, J. Phys. Chem. B 109 (2005) 12394–12398.
[48] S.R. Basu, L.W. Martin, Y.H. Chu, M. Gajek, R. Ramesh, R.C. Rai, X. Xu, J.L. Musfeldt, Appl. Phys. Lett. 92 (2008) 0919051–0919053.
[49] R.V. Pisarev, A.S. Moskvin, A.M. Kalashnikova, T. Rasing, Phys. Rev. B 79 (2009) 23512801–23512816.
[50] A.T. Bell, Science 299 (2003) 1688–1691.
[51] J.W. Tang, Z.G. Zou, J.H. Ye, Chem. Mater. 16 (2004) 1644–1649.
[52] J.G. Yu, J.F. Xiong, B. Cheng, S.W. Liu, Appl. Catal. B 60 (2005) 211–221.
[53] Y.D. Liu, F. Xin, F.N. Wang, S.X. Luo, X.H. Yin, J. Alloys Compd. 498 (2010) 179–184.
[54] J.W. Tang, J.H. Ye, Chem. Phys. Lett. 410 (2005) 104–107.